Generalized Scale: Theory, Algorithms, and Application to Image Inhomogeneity Correction

Anant Madabhushi[a], Jayaram K. Udupa[a], and Andre Souza[a]

[a]Medical Image Processing Group, Department of Radiology
University of Pennsylvania, Philadelphia, PA 19104

ABSTRACT

Scale is a fundamental concept useful in almost all image processing and analysis tasks including segmentation, filtering, interpolation, registration, visualization, and quantitative analysis. Broadly speaking, scale related work can be divided into three categories: (1) multi-scale or scale-space representation, (2) local scale, and (3) locally adaptive scale. The original formulation of scale in the form of scale-space theory came from the presence of multiple scales in nature and the desire to represent measured signals at multiple scales. However, since this representation did not suggest how to select appropriate scales, the notion of local scale was proposed to pick the *right scale* for a particular application from the multi-scale representation of the image. Recently, there has been considerable interest in developing *locally adaptive scales*, the idea being to consider the local size of object in carrying out whatever local operations that are to be done on the image. However, existing locally adaptive models[9,10,7,8] are limited by shape, size, and anisotropic constraints. In this work, we propose a generalized scale model which is adaptive like other local morphometric models, and yet possesses the global spirit of multi-scale representations. We postulate that this *semi-locally* adaptive nature of generalized scale confers it certain distinct advantages over other global and local scale formulations. Further, generalized scale can be easily applied to solve a range of image processing problems. One such problem that we address in this paper is inhomogeneity correction in MR images. We qualitatively and quantitatively demonstrate the superiority of our generalized scale-based correction method over an existing scale-based correction technique,[11] while retaining all the advantages of the existing scale-based method over those published in the literature.

Keywords: Scale, generalized scale, inhomogeneity correction, MRI, Image analysis, Image processing.

1. INTRODUCTION

Scale is a fundamental, well-established concept in image processing. Motivated by the multi-scale nature of real-world images, initial scale related work centered on constructing multi-scale representations such as pyramids[3] and scale-space representations.[1,2] The advantage of traditional scale-space theory is that it ensures that all spatial points and all scales are treated equally and consistently. It does not however directly address the problem of selecting appropriate scales and structures from the multi-scale representation for further analysis. The idea of *local scale* was inspired on account of the problem of picking the *right scale*, which for most applications is not intuitively obvious.[6,4,5]

Local scale formulations however have been geared towards solving specific image processing tasks. Further, since the core idea in these approaches is to extract meaningful scales from a multi-scale representation of the image, they have the problem of causing image smoothing and hence blurring image boundaries. Further, these scale models do not explicitly deal with image structure. Recently, there has been interest in *locally adaptive scales*,[9,10,7,8] the size of which is allowed to change in different parts of the image. The premise behind the concept of locally adaptive scale is to tailor local image operations to local object size. This notion of scale differs from the spirit in which scale is used in scale-space literature, where it typically refers to the size of the σ parameter in the Gaussian kernel and its derivatives. It also differs from the local scale idea in that a homogeneity-based region continuity notion is used in its definition, and it is not affected by locally disconnected nearby structures irrespective of whether they originate from the same object or not.

Correspondence to Jayaram K. Udupa: E-mail: {anantm, jay, andre}@mipg.upenn.edu, Telephone: (215) 662-6780, Fax: (215) 898-9145

Medical Imaging 2004: Image Processing, edited by
J. Michael Fitzpatrick, Milan Sonka, Proceedings of SPIE Vol. 5370
(SPIE, Bellingham, WA, 2004) · 1605-7422/04/$15 · doi: 10.1117/12.535696

A locally adaptive scale model was defined at every image location in[9] as the scale for which the *medialness* measure reaches a local maximum along the scale direction in the scale-space representation. In[7] scale at every voxel was defined as the radius of the largest ball centered at a voxel, such that all voxels within the ball satisfy a pre-defined homogeneity criterion. Similar to this *ball-scale* (from here on abbreviated as *b-scale*), a *tensor scale* model was proposed in,[8] which at every image location was defined as the parametric representation of the largest ellipse (in 2D) or ellipsoid (in 3D) centered at that location and contained in the same homogeneous region under a pre-defined homogeneity criterion. Both b- and tensor scale however are limited by shape and size constraints. While the shape of b- and tensor scale is determined by the choice of the model (ball or ellipse), the largest allowable scale size at any image location for both scale models[7,8] is decided in a somewhat *ad hoc* fashion. The scale model that comes closest in spirit to our formulation is that of Tabb and Ahuja.[10] They define local scale at each image location in terms of a spatial scale parameter that controls a spatial distance function, and a homogeneity scale parameter that controls a homogeneity distance function. These two scale parameters are however tuned for image segmentation, and it is not apparent how or if the model is generalizable to other image processing applications.

The shape and size constraints of these locally adaptive scale models in[7–10] prompt the question: what potential advantages might be gained by removing these constraints? In the present work, we propose a generalized scale model (which we abbreviate as *g-scale* from now on) that is similar to existing locally adaptive scale models[7,8,10] in that it uses a homogeneity-based region continuity criterion for inclusion. It, however, differs from them in that it imposes no shape, size, or anisotropic constraints. We claim that this *semi-locally* adaptive behavior of g-scale confers it certain distinct advantages over other scale formulations. We also propound that g-scale has several interesting properties that greatly simplify its computation and suggest that it has potential utility in several image processing applications. One such application that we address in this paper is background inhomogeneity correction in MR images.

The organization of this paper is as follows. In Section 2 we propose the theory of generalized scale and describe the algorithm for its computation and its properties. In Section 3 we describe our g-scale based correction methodology, and present the results of a qualitative and quantitative comparison with an existing scale based correction method.[11] Finally, in Section 4 we present our conclusions and suggest directions for future work.

2. GENERALIZED SCALE

This section is organized as follows. In Section 2.1, we introduce the concept of g-scale. The algorithm for computing the g-scale is described in Section 2.2. In Section 2.3, we discuss how to select optimal values for the parameters involved in g-scale estimation. Finally, in Section 2.4, we demonstrate qualitatively and quantitatively the robustness of the g-scale estimation process to the presence of scene inhomogeneity.

2.1. Theory and Concepts

Since the idea of g-scale builds on fuzzy connectedness theory,[19,20] before introducing the concept of g-scale, we first present the required preliminaries from fuzzy connectedness.[19,20] The methods propounded in this paper are applicable to n-dimensional images; as such, whenever appropriate our treatment will be n-dimensional.

R^n, Z^n, spels

Let n-dimensional Euclidean space R^n be subdivided into hypercuboids by n mutually orthogonal families of orthogonal hyperplanes.[20] We shall assume, with no loss of generality for our purposes, that the hyperplanes in each family have equal unit spacing so that the hypercuboids are unit hypercubes, and we shall choose coordinates so that the center of each hypercube has integer coordinates. The hypercubes will be called *spels* (an abbreviation for space elements). When n=2 and n=3, the spels are called *pixels* and *voxels*, respectively. The coordinates of a center of a spel are a n-tuple of integers, defining a point in Z^n, and because of this correspondence, the spels will be considered as elements of Z^n.

Fuzzy Adjacency, Hard Adjacency

A fuzzy relation α in Z^n is said to be a *fuzzy adjacency* if it is reflexive and symmetric. We denote by μ_α the

membership function of α in Z^n. The hard adjacency relationships commonly used in digital topology are special cases of fuzzy spel adjacencies. Any hard adjacency relation α_b is a binary relation in Z^n that indicates the adjacency relationship between every two spels in Z^n. In the context of this work, two spels c, $d \in Z^n$ are called α_b-*adjacent*, that is $\mu_{\alpha_b}(c,d) = 1$, if c and d differ in exactly one of their components by 1; otherwise $\mu_{\alpha_b}(c,d)$=0.

Digital Space, Scene, Binary Scene
The pair (Z^n, α_b) is called a *digital space*. A *scene over* Z^n is a pair $\mathcal{C} = (C, f)$ where $C = \{c | -h_j \leq c_j \leq h_j$ for some $h \in {Z^n}_+\}$ (where ${Z^n}_+$ is the set of n-tuples of positive integers) and f is a function whose domain is C and whose range is a set of numbers. We call $\mathcal{C}$ *a binary scene over* Z^n if $\mathcal{C}$ is a scene over Z^n in which the range of f is {0,1}. What is proposed in this paper readily generalizes to *vectorial scenes* in which f is vector valued.

Fuzzy Affinity
A fuzzy relation κ in C is said to be a *fuzzy spel affinity* in $\mathcal{C}$ if it is reflexive and symmetric. The strength of the fuzzy affinity κ in C is denoted by μ_κ. In practice, we would want κ to be such that $\mu_\kappa(c,d)$ is a function of $\mu_\alpha(c,d)$ and of $f(c)$ and $f(d)$. That is, we would want the strength of affinity between spels c and d to depend on how near they are spatially and on how near they are based on their intensity features. Below is one functional form of $\mu_\kappa(c,d)$ that captures the degree of local hanging togetherness of c and d based on intensity homogeneity.

$$\mu_\kappa(c,d) = \mu_\alpha(c,d)\mu_\psi(c,d), \tag{1}$$

where μ_ψ represents the *homogeneity-based component* of affinity and indicates how similar the intensities of c and d are. We assume that the homogeneity between two spels c and d in a scene $\mathcal{C}$=(C, f) can be characterized by $|f(c) - f(d)|$ and express $\mu_\psi(c,d)$ as some function (W_ψ) of $|f(c) - f(d)|$.

$$\mu_\psi(c,d) = W_\psi(|f(c) - f(d)|) \tag{2}$$

Path, α_b-Path
Any *path* $\mathbf{p}_{cd}$ in $\mathcal{C}$ from a spel $c \in C$ to a spel $d \in C$ is any sequence $< c^{(1)}, c^{(2)}, ..., c^{(m-1)}, c^{(m)} >$ of spels, $m \geq 2$, all in C, such that $c^{(1)}$=c and $c^{(m)}$=d. For any set $S \subset C$, and spels $c, d \in S$, the sequence $< c^{(1)}, c^{(2)}, ..., c^{(m-1)}, c^{(m)} >$ of elements in S is said to be an α_b-*path* p_{cd} *in* S *connecting* c *to* d if $c^{(1)} = c, c^{(m)} = d$, and, for $1 \leq i < m$, $\mu_{\alpha_b}(c^{(i)}, c^{(i+1)})$=1.

DEFINITION 1. For any scene $\mathcal{C} = (C, f)$, spel $c \in C$, for any affinity κ in $\mathcal{C}$, and for any number $\theta \in [0, 1]$, the *g-scale* $G_\theta(c)$ *of spel* c *in* $\mathcal{C}$ is the largest subset of C such that
(1) $G_\theta(c)$ contains c, and
(2) for any spels $d, o \in G_\theta(c)$, there exists an α_b-path $p_{do} =< c^{(1)} = d, c^{(2)}, ..., c^{(m-1)}, c^{(m)} = o >$, where, for all $1 \leq i \leq m$, $c^{(i)} \in G_\theta(c)$ and for all j, $1 \leq j \leq m-1$, $\mu_\psi(c^{(j)}, c^{(j+1)}) \geq \theta$.

The functional form that we use for the homogeneity component μ_ψ is a zero-mean un-normalized Gaussian function with a standard deviation of σ_ψ. Note, that even when the functional form of W_ψ is a step function, $G_\theta(c)$ does not represent a thresholded connected component.

DEFINITION 2. For any scene $\mathcal{C}$=(C, f), for any affinity κ in $\mathcal{C}$, and for any number θ=$[0, 1]$, the *g-scale set* $\mathcal{G}_\theta(\mathcal{C})$ *of scene* $\mathcal{C}$ is defined as $\mathcal{G}_\theta(\mathcal{C})$=$\{G_\theta(c) | c \in C\}$. For the rest of this paper, we will refer to $G_\theta(c)$ also as the g-scale region associated with spel c. $G_\theta(c)$ has some interesting properties. The most important for our purposes is given in the following theorem.

THEOREM 1. For any scene $\mathcal{C}$=(C, f), for any spel $d \in G_\theta(c)$, for any affinity $\kappa \in \mathcal{C}$, and for any number θ =[0,1], $G_\theta(d)$=$G_\theta(c)$.

2.2. Algorithm for computing g-scale

Theorem 1 above implies that once the g-scale $G_\theta(c)$ for a spel c has been computed, one does not need to compute the g-scale $G_\theta(d)$ for any other spel $d \in G_\theta(c)$. This has obvious implications in terms of reducing computational time. This idea forms the core of the algorithm presented below for computing g-scale over a given scene.

Algorithm $GS1$

Input: $\mathcal{C}$, θ, κ
Output: $\mathcal{G}_\theta(\mathcal{C})$
Auxiliary Data Structures: A que Q.

begin
0. unmark all spels of C;
1. *repeat*
2. take an unmarked spel c of C and put it in Q;
3. mark c and set $G_\theta(c)$ to empty;
4. *while* Q is not empty *do*
5. remove a spel d from Q and add it to $G_\theta(c)$;
6. *for* each unmarked spel e α_b-adjacent to d *do*
7. *if* $\mu_\kappa(d,e) \geq \theta$ *then* put e in Q and mark it;
8. *endfor*;
9. *endwhile*;
10. output $G_\theta(c)$;
11. *until* there is no unmarked spel in C;

end

2.3. Selecting optimal values for g-scale parameters

For a given scene $\mathcal{C}=(C,f)$, since the g-scale set $\mathcal{G}_\theta(\mathcal{C})$ over $\mathcal{C}$ is dependent on the region-homogeneity parameter σ_ψ and the threshold θ, we need to determine optimal values for these parameters that will result in a visually meaningful and useful g-scale $\mathcal{G}_\theta(\mathcal{C})$. We use the automated method described in[7] to select a proper value of σ_ψ. This involves computing the standard deviation σ_h of local intensity gradients directly from the local in-plane gradients in the scene. The value of σ_ψ is then set as

$$\sigma_\psi = \zeta \sigma_h, \tag{3}$$

where ζ controls the width of the homogeneity function W_ψ. Selecting a higher value for ζ implies that two α_b-adjacent spels can have a larger intensity difference and yet be considered to belong to the same g-scale region. Similarly, a higher value of θ implies that two α_b-adjacent spels must have very similar intensities in order for them to belong to the same g-scale region. Figures 1(b)-(f) are the g-scale sets $\mathcal{G}_\theta(\mathcal{C})$ resulting from different combinations of values of θ and ζ for the original scene depicted in Figure 1(a). In order to display $\mathcal{G}_\theta(\mathcal{C})$, all spels in a g-scale region in $\mathcal{G}_\theta(\mathcal{C})$ were assigned a single color. Every $G_\theta \in \mathcal{G}_\theta(\mathcal{C})$ was represented by a unique color. As reflected in Figures 1(e) and (f), higher values of θ and lower values of ζ cause more severe partitioning, while lower values of θ and higher values of ζ result in a smaller number of larger g-scale regions (Figure 1(b)). The values of ζ and θ used for computing $\mathcal{G}_\theta(\mathcal{C})$ in Figures 1(c) and (d) yield visually meaningful partitions of the scene.

Deciding on optimal values for ζ and θ is thus a tradeoff between a large number of very small g-scale regions, each of which represent a single tissue region, or a small number of large g-scale regions, each of which may represent a mixture of different tissue regions. The selection of parameter values is thus motivated by (1) obtaining g-scale regions which represent a single dominant tissue region and (2) obtaining a meaningful partitioning of the scene domain.

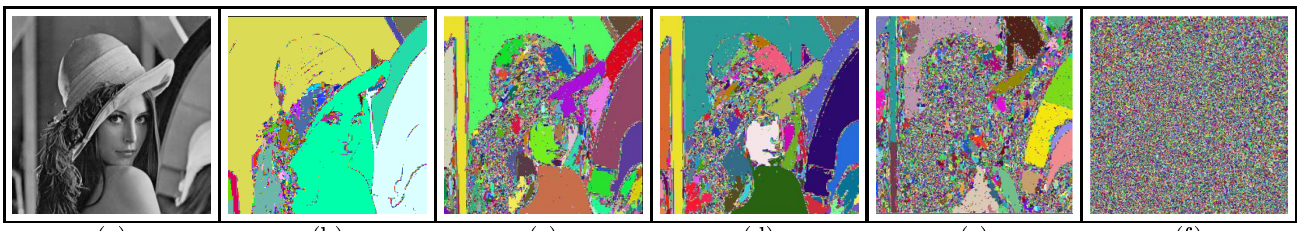

(a) (b) (c) (d) (e) (f)

Figure 1. (a) Original scene ($\mathcal{C}$) and $\mathcal{G}_\theta(\mathcal{C})$ corresponding to (b) θ=0.8, ζ=3.0, (c) θ=0.94, ζ=2.0, (d) θ=0.94, ζ=2.5, (e) θ=0.98, ζ=0.5, (f) θ=0.98, ζ=0.

In order to select appropriate parameter values, we performed the following experiment. We began with a set of clinical MRI scenes of the brain, for which segmented white matter (WM) and gray matter (GM) masks are available. For different values of ζ and θ, we computed the g-scale set over the given scenes. For the 100 largest g-scale regions we computed the average purity (percentage of the largest dominant tissue in a g-scale region). Those values of ζ and θ were selected which provided a reasonable tradeoff between high purity and a lower number of g-scale regions.

2.4. Effect of inhomogeneity on the estimation of g-scale

Since we are interested in applying g-scale to the problem of inhomogeneity correction, we evaluated the effect of inhomogeneity on the estimation of g-scale. We did this by introducing varying levels of different models of background inhomogeneity into a scene and computing the corresponding g-scale sets over the different scenes containing inhomogeneity. Starting with the original scene $\mathcal{C}_1=(C, f_1)$ with no inhomogeneity, the scene $\mathcal{C}_2=(C, f_2)$ containing inhomogeneity is given by,

$$f_2(c) = f_{bt}(c) f_1(c), \tag{4}$$

where $f_{bt}(c)$ is taken to be a ramp or a Gaussian function. We defined a figure of merit (FOM) $\mathcal{F}$ to quantitatively compare the difference between the g-scale set $\mathcal{G}_\theta(\mathcal{C}_1)$=$\{G^1_{\theta 1}, G^1_{\theta 2}, \ldots, G^1_{\theta m_1}\}$ over $\mathcal{C}_1$, and the g-scale set $\mathcal{G}_\theta(\mathcal{C}_2)$=$\{G^2_{\theta 1}, G^2_{\theta 2}, \ldots, G^2_{\theta m_2}\}$ over $\mathcal{C}_2$, where m_1 and m_2 are the cardinality of $\mathcal{G}_\theta(\mathcal{C}_1)$ and $\mathcal{G}_\theta(\mathcal{C}_2)$, respectively.

$$\mathcal{F}(\mathcal{G}_\theta(\mathcal{C}_1), \mathcal{G}_\theta(\mathcal{C}_2)) = \frac{1}{2m_1} \sum_{i=1}^{m_1} \sum_{j=1}^{m_2} \frac{\lambda_i}{|\, G^1_{\theta i} \cup G^2_{\theta j} \,|} + \frac{1}{2m_2} \sum_{j=1}^{m_2} \sum_{i=1}^{m_1} \frac{\lambda_j}{|\, G^1_{\theta i} \cup G^2_{\theta j} \,|} \tag{5}$$

where λ_i=$\max_j\{|\, G^1_{\theta i} \cap G^2_{\theta j} |\}$ and λ_j=$\max_i\{|\, G^1_{\theta i} \cap G^2_{\theta j} \,|\}$. The rationale behind our choice of $\mathcal{F}$ is to determine pairs of g-scale regions in $\mathcal{G}_\theta(\mathcal{C}_1)$ and $\mathcal{G}_\theta(\mathcal{C}_2)$ that have maximum overlap. Hence, the larger the number of pairs of g-scale regions in $\mathcal{G}_\theta(\mathcal{C}_1)$ and $\mathcal{G}_\theta(\mathcal{C}_2)$ that have a high degree of overlap, the more similar $\mathcal{G}_\theta(\mathcal{C}_1)$ and $\mathcal{G}_\theta(\mathcal{C}_2)$ will be, and higher is the value of $\mathcal{F}(\mathcal{G}_\theta(\mathcal{C}_1), \mathcal{G}_\theta(\mathcal{C}_2))$.

In Figures 2(a)-(d) are shown scenes in which artificial inhomogeneity has been introduced and Figures 2(e)-(h) show the corresponding $\mathcal{G}_\theta(\mathcal{C})$, all computed by using the same value of ζ and θ. In table 1 are shown the FOM values for the scene in Figure 2 for three levels of Gaussian and ramp variations. The high $\mathcal{F}$ values and the similarity among the displays in Figures 2(e)-(h) indicate that the estimation of g-scale is resistant to the presence of different models and levels of background inhomogeneity.

3. INHOMOGENEITY CORRECTION

Intensity non-uniformity is a serious problem in many image processing areas. In MRI, this may be caused by a number of different factors, including poor RF coil uniformity, static field inhomogeneity, RF penetration, gradient-driven eddy currents, and patient anatomy both inside and outside the field of view. Although these

Level of Inhomogeneity	Ramp	Gaussian
Low	.9584	.9716
Moderate	.9369	.9211
High	.9278	.8741

Table 1. Values of $\mathcal{F}$ for the lena image for three levels of ramp and Gaussian background variations.

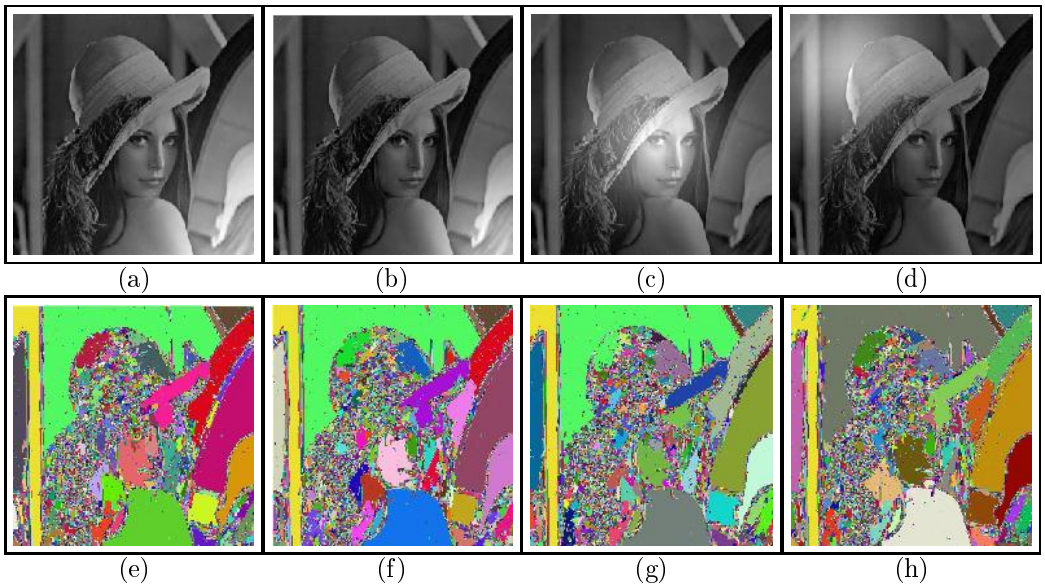

Figure 2. (a)-(b) Scene with low and moderate levels of ramp backround variation. (c) Scene with a high level of Gaussian background variation centered at the center of the scene domain. (d) Scene with a moderate level of Gaussian background variation centered at the upper left corner of the scene domain. (e)-(h) $\mathcal{G}_\theta(\mathcal{C})$ for scenes in (a)-(d).

intensity variations may usually have little impact on visual diagnosis, they can significantly affect the performance of many image processing, segmentation, and analysis techniques. A robust, inexpensive, general, and scanner- and protocol-independent means of correcting this artifact is essential for such processing techniques to have acceptable precision, accuracy, and efficiency. For MR images, the observed signal intensity at any voxel is the product of the true signal intensity and the inhomogeneity at that point. Hence, a correction technique requires an estimate of the scene inhomogeneity which in turn requires an estimate of the true signal intensity. Several methods of inhomogeneity correction have been proposed since the first paper on the subject.[12] In[12] an estimate of the true signal intensity within a local window was obtained based on the assumption that the mean or median intensity within a local window would be equal to the global mean or median if there is no inhomogeneity in the image. This assumption is however not valid for most cases and is only approximately true for large window sizes. Other correction methods have been proposed which seek to obtain an accurate estimate of the true tissue signal intensity, based either on some training[14] or by using some *a-priori* information about the data set.[13,17] Others require manual intervention to segment the tissue regions.[15,16] In[11] a fully automated b-scale-based correction methodology was proposed. The assumption of this methodology was that the area represented by the union of the largest scale regions corresponds roughly to the largest tissue region in the image. The average intensity within this thresholded region was then used as an estimate of the true tissue intensity. One limitation of using b-scale to estimate scene inhomogeneity is that since it ignores local anisotropy and orientation, it is not very effective along elongated structures and edges. More importantly,

however, thresholding by itself cannot guarantee a sufficiently large region of the same tissue. The g-scale based approach seems to be able to overcome many of the issues related to inhomogeneity correction. We believe that this approach is superior to existing methodologies on account of the following reasons:
(1) g-scale has the inherent property of not being affected by slow background variations. This is mainly because it inherits the properties of fuzzy connectedness,[7,19] which has demonstrated as to how slow varying background intensity non-uniformity does not affect tracking of the same object region.
(2) g-scale results in an automatic partitioning of the scene into a number of homogeneous regions; each homogeneous region corresponds to a single tissue region along with its attendant inhomogeneity. Hence, without explicit segmentation and with no *a priori* knowledge about the MRI protocol used, body region imaged, or the scanner used, it is possible to sample the same tissue region, and hence, to accurately estimate true tissue intensities.
(3) The largest g-scale region is perhaps our best hope of estimating true tissue intensities, and hence inhomogeneities, at points well distributed over the scene domain. This, we believe, is a pre-requisite to a good estimate of the inhomogeneity function by any method.

The rest of this section is organized as follows. In Section 3.1, we introduce the notation, and describe our methodology in Section 3.2. In Section 3.3, we present the results of qualitatively and quantitatively comparing the g-scale correction method with an existing b-scale method.[11]

3.1. Terminology

We will use the following notation in the rest of this section.

$\mathcal{C}$=(C,f): a given scene corrupted by background variation.
$\mathcal{C}_{bt}$=(C,f_{bt}): the true background variation component in $\mathcal{C}$.
$\mathcal{C}_u$=(C,f_u): $\mathcal{C}$ without the background variation component $\mathcal{C}_{bt}$.
$\mathcal{C}_b$=(C,f_b): the scene resulting from applying the b-scale correction method to $\mathcal{C}$.
$\mathcal{C}_g$=(C,f_g): the scene resulting from applying the g-scale correction method to $\mathcal{C}$.
$\mathcal{C}_{bg}$=(C,f_{bg}): the background variation component in $\mathcal{C}$ estimated by the g-scale correction method.
$\mathcal{C}_{bb}$=(C,f_{bb}): the background variation component in $\mathcal{C}$ estimated by the b-scale correction method.

3.2. Methodology

For an MRI scene, the inhomogeneity at any spel $c \in C$ can be expressed as,

$$f_{bt}(c) = \frac{f(c)}{f_u(c)}. \tag{6}$$

The central idea of most correction methodologies is thus to estimate $f_{bt}(c)$ by obtaining a good estimate of the true scene intensity $f_u(c)$. In our methodology we use g-scale to obtain an accurate estimate of $f_u(c)$. The steps in our approach are as follows:

1. Determine the foreground region of $\mathcal{C}$ as only those spels whose intensity is higher than the average scene intensity. All subsequent computations are confined to this region.

2. Compute the g-scale set $\mathcal{G}_\theta(\mathcal{C})$=$\{G_{\theta 1}, G_{\theta 2},...,G_{\theta m}\}$, over all foreground spels in $\mathcal{C}$.

3. Determine the largest g-scale region $G_\theta^{\max}$=$\max_{G_{\theta i} \in \mathcal{G}_\theta(\mathcal{C})}[|G_{\theta i}|]$ in the g-scale set $\mathcal{G}_\theta(\mathcal{C})$. The maximum intensity $f_{\max}$, in $G_\theta^{\max}$ is determined as,

$$f_{\max} = \max_{c \in G_\theta^{\max}}[f(c)]. \tag{7}$$

If the maximum value of f_{bt} over the scene domain is 1, then f_{max} gives a closer estimate of true intensity within $G_\theta^{\max}$. We then estimate the background variation component $f_{bg}(c)$ for all spels $c \in G_\theta^{\max}$ as

$$f_{bg}(c) = \frac{f(c)}{f_{\max}}. \tag{8}$$

4. A 2^{nd} order polynomial $p(c)$ is fit to this estimated background variation and correction is performed by,

$$f_g(c) = \frac{f(c)}{p(c)}. \tag{9}$$

5. The entire process from Step 2 to Step 4 is repeated iteratively until the size of $G_\theta^{\max}$ does not change considerably from one iteration to the next.

3.3. Results

For the purpose of qualitative evaluation, we tested the b- and g-scale correction methods on a number of clinical MR images acquired during routine scanning and corresponding to different MR protocols and body parts. The scenes resulting from the application of the two methods were then visually inspected for residual inhomogeneity. The two methods were also quantitatively compared on a total of 90 phantom scenes from the MNI data base,[18] corresponding to normal and multiple sclerosis (MS) brains. These data sets correspond to the PD, T1, and T2 protocols, five different slice thickness values, and three levels of background inhomogeneity (0%, 20%, 40%), corresponding to no, mild, and severe inhomogeneity levels, respectively. The scenes resulting from the application of the two methods were quantitatively evaluated to determine the residual inhomogeneity.

3.3.1. Qualitative

In Figure 3 are shown slices from three clinical MRI scenes corresponding to different parts of the human body and the results obtained from the b- and g-scale correction methods. Figure 3(a) shows a slice from a clinical MRI scene of the thorax, corrupted by severe inhomogeneity. The result after g-scale correction in Figure 3(c) not only corrects for most of the inhomogeneity in Figure 3(a), but also reveals significantly more anatomic detail than the corresponding result obtained by b-scale correction (Figure 3(b)). Even for scenes with mild inhomogeneity, as in the MRI scene of the foot (Figure 3(d)) g-scale correction (Figure 3(f)) out-performs b-scale correction (Figure 3(e)). Note in a slice from the b-scale corrected MR scene of the shoulder joint (Figure 3(h)), the introduction of a noise artifact in the lower right corner of the slice display. Note also that the result of g-scale correction in Figure 3(i) does not produce this noise artifact and reveals image details obfuscated by inhomogeneity in the original scene (Figure 3(g)) as well as in the result of b-scale correction.

3.3.2. Quantitative

Different measures have been used for evaluating the effectiveness of correction procedures. In,[21] we used the percent coefficient of variation to measure residual inhomogeneity in clinical images. Since, for phantom scenes the true signal intensity is known, we decided to use the root mean squared (RMS) difference error between the original and corrected scenes as the figure of merit.

We quantitatively compared the original MNI phantom scenes (0% inhomogeneity), with the results of b- and g-scale correction for three levels of inhomogeneity (0%, 20%, 40%). The reason for including scenes with no inhomogeneity (0%) in this evaluation is as follows. Ideally a correction algorithm should be expected to leave a scene containing no inhomogeneity unchanged. Hence, the RMS difference between the original scenes (0% inhomogeneity) and the scenes obtained by the application of a particular correction method would be an indicator of the amount of artificial inhomogeneity introduced into the original scene by that correction method.

In Tables 2, 3, and 4 are the RMS values for the results of b- and g-scale correction for normal and MS brains and for the PD, T1, and T2 protocols. All scenes were standardized by using the method in[22] prior to evaluation but following inhomogeneity correction.[21] In 96.7% of the cases, g-scale outperformed the b-scale correction method. In only three out of a total of 90 scenes did the b-scale method outperform the g-scale correction technique. A paired t-test on each of the 18 sets of RMS values from the b- and g-scale correction methods, indicated that the difference in RMS values was statistically significant ($p \leq 0.05$) in all 18 cases in favor of the g-scale method. The reason for the superior performance of the g-scale method can be gleaned from Figure 4 which shows the result of the two methods on a slice from a MNI PD phantom scene of the brain. Figures 4(a)-(d) show the same slices from the scenes corresponding to $\mathcal{C}_u$, $\mathcal{C}$, $\mathcal{C}_b$, and $\mathcal{C}_g$. Figure 4(e) represents the largest g-scale region extracted from the g-scale set over $\mathcal{C}$ that is used to estimate the inhomogeneity scene $\mathcal{C}_{bg}$ (Figure 4(h)). The similarity between $\mathcal{C}_{bg}$ and the true inhomogeneity $\mathcal{C}_{bt}$ (Figure 4(f)) explains why $\mathcal{C}_g$ (Figure 4(d)) contains significantly less residual inhomogeneity than $\mathcal{C}$ and $\mathcal{C}_b$ (Figures 4(b), (c)).

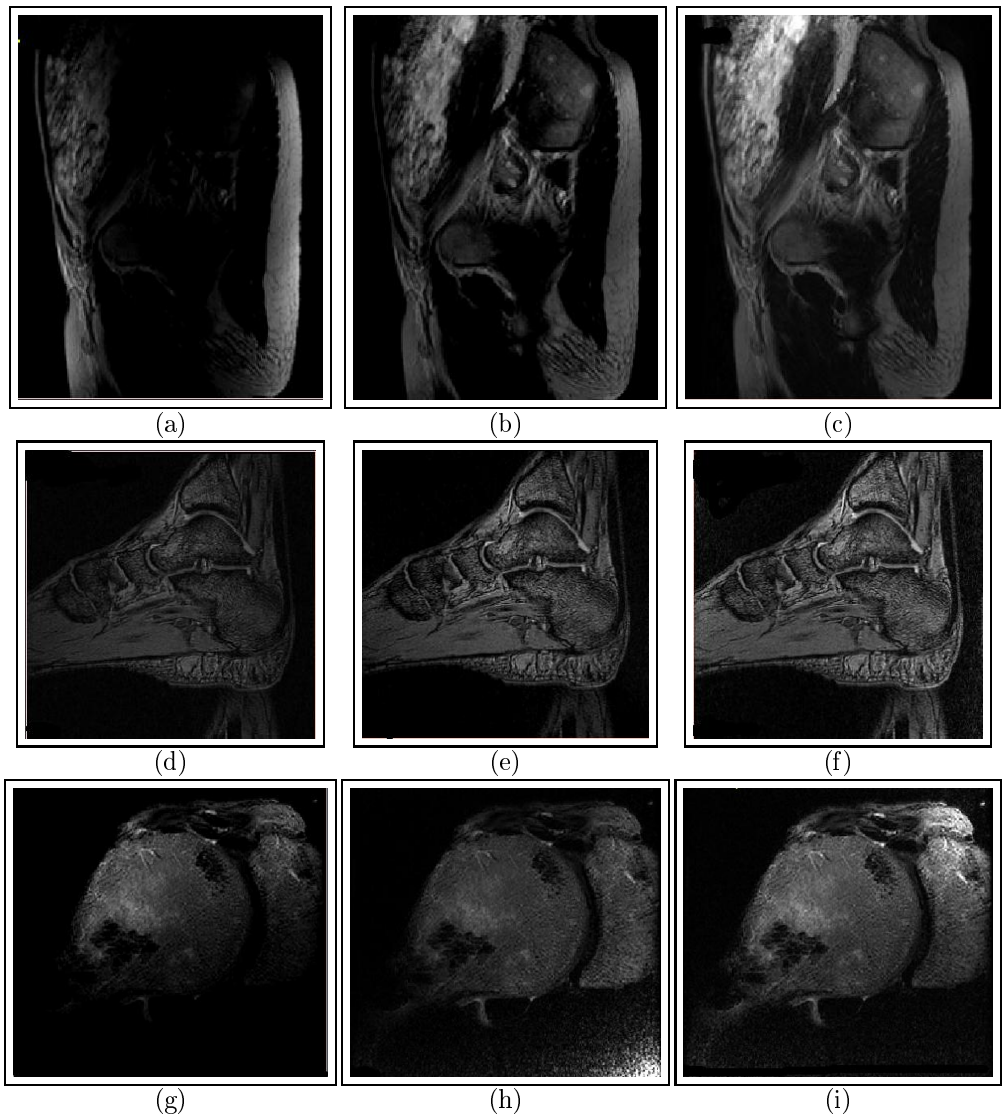

Figure 3. (a), (d), (g) Slices from the original MR scene; (b), (e), (h) corresponding slices from the b-scale corrected scene; (c), (f), (i) corresponding slices from the g-scale corrected scenes.

4. CONCLUDING REMARKS

In this paper, we have presented a novel semi-locally adaptive scale model called g-scale that is not limited by shape or size constraints. The model has some nice theoretical properties that makes it easy to compute. The g-scale requires only two parameters, both of which can be easily estimated without any *a priori* knowledge about the scene. Further, since g-scale inherits the properties of fuzzy connectedness,[7,19] it has the inherent property of being resistant to the presence of inhomogeneity in a scene. Importantly, unlike other local scale models, g-scale can be easily applied to solve different image processing tasks, one of which - inhomogeneity correction - we addressed in this paper.

The g-scale based correction method was quantitatively and qualitatively compared with an existing scale-based correction technique.[11] It was found to be superior to the b-scale method on clinical and phantom images, across protocols and levels of inhomogeneity. Further, considering the artifacts introduced by the correction

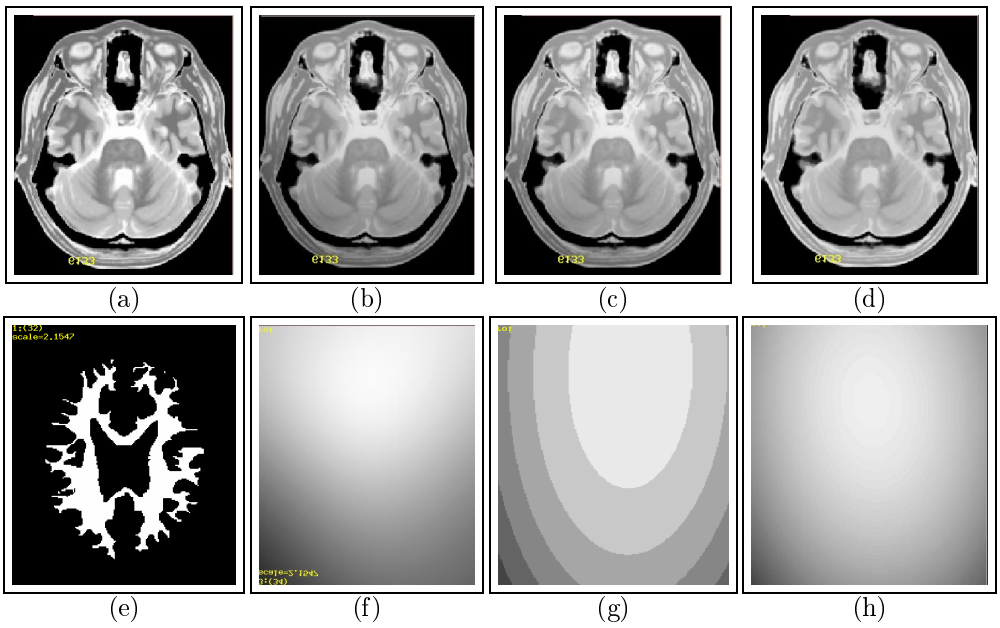

Figure 4. Displays of the same slice from a normal MNI PD brain scene for various situations. (a) $\mathcal{C}_u$, (b) $\mathcal{C}$ with 40% inhomogeneity, (c) $\mathcal{C}_b$, (d) $\mathcal{C}_g$, (e) $G_\theta^{\max}$, (f) $\mathcal{C}_{bt}$, (g) $\mathcal{C}_{bb}$, (h) $\mathcal{C}_{bg}$.

	Normal						MS					
	b-Scale			g-Scale			b-Scale			g-Scale		
mm	0%	20%	40%	0%	20%	40%	0%	20%	40%	0%	20%	40%
1	0.305	3.634	5.855	0.143	1.857	2.155	0.213	1.897	6.194	0.903	1.451	1.770
3	0.381	3.376	5.026	0.188	1.971	3.005	0.136	1.873	5.532	0.964	1.736	2.603
5	0.139	1.931	5.058	0.182	1.971	3.005	0.132	2.782	5.326	0.115	1.129	2.923
7	0.168	2.145	4.690	0.182	1.483	2.720	0.159	3.634	5.241	0.144	1.009	2.817
9	0.247	2.358	4.586	0.164	2.007	3.301	0.239	3.222	5.121	0.126	1.001	2.949

Table 2. RMS values for three levels of inhomogeneity for Phantom PD scenes.

process, g-scale seems to be superior to b-scale. When correction was performed on scenes containing 0% inhomogeneity, g-scale correction was found to alter the original scenes significantly less than b-scale correction. We attribute the reason for the superior performance of g-scale to the fact that it results in a segmentation of the scene into larger homogeneous tissue regions that include the inhomogeneity. This allows us to approximate the true inhomogeneity better than in the b-scale case as illustrated in Figures 4(g) and (h).

In future work, we will study the use of g-scale in other image processing applications such as image filtering, intensity standardization, segmentation, and visualization.

ACKNOWLEDGMENTS

This work was supported by a DHHS grant NS37172. The authors are grateful to Punam Saha and Jiamin Liu for some early discussions on g-scale.

REFERENCES

1. A.P. Witkin, "Scale-space filtering", *Intl. Conf. on Artifical Intell.*, pp. 1019-22, 1983.

	Normal						MS					
	b-Scale			g-Scale			b-Scale			g-Scale		
mm	0%	20%	40%	0%	20%	40%	0%	20%	40%	0%	20%	40%
1	0.301	1.164	2.072	1.660	0.755	1.561	0.260	1.171	2.039	0.153	0.856	1.572
3	0.483	1.291	2.518	0.255	0.830	1.689	0.315	1.244	1.803	0.216	0.826	1.690
5	1.726	1.781	3.770	0.281	0.965	1.816	0.451	1.592	2.719	0.242	0.933	1.806
7	1.643	2.281	5.001	0.269	0.946	1.967	0.586	1.819	3.790	0.273	0.947	1.998
9	1.643	3.106	6.402	0.217	0.984	2.192	0.673	1.289	5.670	0.235	1.018	2.106

Table 3. RMS values for three levels of inhomogeneity for Phantom T1 scenes.

	Normal						MS					
	b-Scale			g-Scale			b-Scale			g-Scale		
mm	0%	20%	40%	0%	20%	40%	0%	20%	40%	0%	20%	40%
1	0.221	4.824	8.195	0.127	1.143	1.764	0.231	4.108	6.376	0.132	1.964	2.108
3	0.556	6.215	8.695	0.114	0.974	1.680	0.524	4.771	6.379	0.127	2.067	2.701
5	0.288	5.721	8.400	0.124	1.467	2.041	0.649	5.186	6.451	0.126	1.334	2.909
7	0.932	6.715	7.823	0.115	1.545	2.202	0.817	3.498	6.952	0.136	1.575	3.094
9	1.059	6.468	7.429	0.126	2.053	2.307	1.145	2.976	6.929	0.139	1.862	3.249

Table 4. RMS values for three levels of inhomogeneity for Phantom T2 scenes.

2. J. J. Koenderink and A. J. van Doorn, "Representation of local geometry in the visual system", *Biological Cybernetics*, vol. 55, pp. 367-75, 1987.
3. P. Burt, "Fast Filter Transform for Image Processing", *Computer Graphics and Image Processing*, pp. 20-51, 1981.
4. J. H. Elder and S.W. Zucker, "Local scale control for edge detection and blur estimation ", *IEEE Trans. on Pattern Recog. and Machine Intelligence*, vol. 20[7], pp. 699-716, 1998.
5. J. Plantier, S. Lelandais, and L. Boutte, "A Shape from Texture method based on Local Scales Extraction: Precision and Results", *Intl. Conf. on Image Processing*, vol. 2, pp. 261-264, 2001.
6. T. Lindeberg, "Automatic Scale Selection as a Pre-Processing Stage for Interpreting the Visual World", *Proc. of Fund. Structural Properties in Image and Pattern Analysis*, vol. 130, pp. 9-23, 1999.
7. P. K. Saha, J. K. Udupa, and D. Odhner "Scale-based Fuzzy Connected Image Segmentation: Theory, Algorithms, and Validation", *CVIU*, vol. 77, pp. 145-174, 2000.
8. P. K. Saha, "Novel Theory and Methods for Tensor Scale: A Local Morphometric Parameter", *Proceedings of SPIE: Medical Imaging*, vol. 2, pp. 314-24, 2003.
9. S. M. Pizer, D. Eberly, and D. S. Fritsch, "Zoom-invariant vision of figural shape: the mathematics of core", *CVIU*, vol. 69, pp. 55-71, 1998.
10. M. Tabb and N. Ahuja, " Multiscale image segmentation by integrated edge and region detection ", *IEEE Trans. on Image Processing*, vol. 6[5], pp. 642-655, 1997.
11. Y. Zhuge, J. Udupa, J. Liu, P. K. Saha "A Scale-Based method for correcting background intensity variation in acquired images", *Proceedings of SPIE: Medical Imaging*, vol. 4684, pp. 1103-1111, 2002.
12. L. Axel, J. Constantini, and J. Listerud, "Intensity Correction in Surface-Coil MR Imaging", *American Journal of Radiol.*, vol. 148, pp. 418-420, 1987.
13. W. Wells, W. Grimson, R. Kiknis, and F. A. Jolez, "Adaptive Segmentation of MRI data", *IEEE Trans. on Med. Imaging*, vol. 15, pp. 429-443, 1996.
14. M. Styner, C. Brechbuhler, G. Szekely and G. Gerig, "Parametric Estimate of Intensity Inhomogeneities Applied to MRI", *IEEE Trans. on Med. Imaging*, vol. 19, pp. 153-165, 2000.
15. B. M. Dawant, A. P. Zjidenbos, and R. A. Margolin, "Correction of intensity variations in MR images for computer-aided tissue classification", *IEEE Trans. on Med. Imaging*, vol. 12, pp. 770-81, 1993.
16. C. R. Meyer, P. H. B. Land, and J. Pipe, "Retrospective Correction of intensity inhomogeneities in MRI", *IEEE Trans. on Med. Imaging*, vol. 14, pp. 36-41, 1995.

17. K. Leemput, F. Maes, D. Vandermeulen and P. Suetens, "Automated Model-Based Bias Field Correction of MR Images of the Brain", *IEEE Trans. on Med. Imaging*, vol. 18, pp. 885-896, 1999.
18. C.A. Cocosco, V. Kollokian, R.K.-S. Kwan, A.C. Evans, "BrainWeb: Online Interface to a 3D MRI Simulated Brain Database", *NeuroImage*, vol.5, no.4, part 2/4, S425, 1997.
19. J. K. Udupa, S. Samarasekera, "Fuzzy Connectedness and Object Definition: Theory, Algorithms, and Applications in Image Segmentation", *CVGIP: Graphical Model and Image Processing*, vol. 58(3), pp. 246-61, 1996.
20. J. K. Udupa, "Multidimensional Digital Boundaries", *CVGIP: Graphical Models and Image Processing*, vol. 56[4], pg 311-323, 1994.
21. A. Madabhushi and J. Udupa, "Interplay of Intensity Standardization and Inhomogeneity Correction in MR Image Analysis", *Proceedings of SPIE: Medical Imaging*, vol. 4[23], pp. 772-783, 2003.
22. L. G. Nyul and J. K. Udupa, "On standardizing the MR Image Intensity Scale", *Magnetic Resonance in Medicine*, vol. 42, pp. 1072-1081, 1999.